Int. J. Heat Mass Transfer. Vol. 34, No. 9, pp. 2373–2385, 1991
Printed in Great Britain

0017-9310/91 $3.00+0.00

Coherent structure of turbulent longitudinal vortices in unstably-stratified turbulent flow

KEISUKE FUKUI and MASAMOTO NAKAJIMA
Department of Chemical Engineering, Himeji Institute of Technology, Himeji 671-22, Japan

and

HIROMASA UEDA
Research Institute for Applied Mechanics, Kyushu University, Kasuga 816, Japan

(*Received* 6 *September* 1990 *and in final form* 19 *November* 1990)

Abstract—The large-scale coherent structure in a density-stratified turbulent flow under strongly unstable conditions is investigated experimentally by using some conditional sampling techniques. An array of the large-scale longitudinal vortical rolls can be recognized by using the new conditional sampling technique, that is, the thermal-plume (TP) detecting one to single out the hot or cold thermal plume at the boundary of ordered turbulent rolls. The conditional sampling measurements provide the detailed knowledge of the fine structure of turbulence and the mechanics of turbulent heat and momentum transfers.

1. INTRODUCTION

EXPERIMENTAL studies on the organized structure of the intermittent 'bursting' phenomenon, which is a main contributor to all turbulence production near the wall, have been carried out by a number of investigators from visual observations [1–4] and from conditionally sampled measurements [5–10]. Recently, many numerical analyses of a large eddy simulation (LES) and a direct numerical simulation (DNS) of the Navier–Stokes equation have been successfully applied to a variety of turbulent flows. These experimental and numerical studies have contributed significantly to recent studies on the turbulent structure of neutral flows without buoyancy effects. In the presence of density variation in a fluid layer, it is considered that the buoyancy force or stratification effect causes the essential changes of turbulence structure and also of turbulent transport mechanics.

The stratified turbulent flows have been studied extensively by many meteorologists and oceanographers on the basis of field observations. Some laboratory studies have been carried out using specially-designed wind tunnels and other facilities [11–15] to obtain reliable data and to understand in more detail the stratification effects on turbulence structure. As to the unstably-stratified flow, Nicholl [14] measured the instantaneous velocity and temperature in the fully-turbulent boundary layer over a heated horizontal floor and examined the dynamical buoyancy effects of a sudden increase in the floor temperature on turbulent structure. He suggested that a strong discontinuity in the floor temperature caused the fine-scale motion of convective columns, which were organized at the interface between the hot and cold fluid layers. Since the fine-scale convective columns violently rose, the mean pressure near the wall was significantly reduced and then a local wall jet was generated immediately downstream of the surface temperature discontinuity. Townsend [15] also examined the turbulent boundary layer over a heated horizontal plane and proposed the similarity of mean velocity and temperature profiles, together with turbulent intensity profiles on the basis of his concept of the viscous-conduction layer. He also tried to explain the validity of the similarity, based upon the situation that the nearly two-dimensional plumes in the form of long eddies, with axes aligned in the flow direction ejected from the viscous layer in the vicinity of the floor, losing heat to the surrounding fluid, and the emergent plume were broken up in the transition region by general turbulent motion.

The new similarity of velocity, temperature and turbulent intensities was proposed in refs. [16, 17], where the 'local gradient model', which was ensured from the measurements established in a fully-developed stratified flow by using a long rectangular duct with large aspect ratio. The results, based on the local gradient model, agreed with observations by Businger *et al.* [18]. As to a similarity of turbulent diffusion of passive-scalar quantity, the present authors [19] also showed that the ratio of lateral and vertical eddy diffusion coefficients could be correlated by only the Monin–Obukhov length. Using conditional sampling measurements of turbulent quantities, the remarkably different effects of unstable stratification on turbulent structure in the wall and outer regions were shown [20], and the correlation

NOMENCLATURE

g	gravitational acceleration [m s^{-1}]
H	threshold [—]
h	height of duct [m]
R_a	auto-correlation coefficient [—]
R_s	space-correlation coefficient [—]
Re	Reynolds number, $2U_{av}h/\nu$ [—]
$\overline{Ri}$	bulk Richardson number, $g\beta\Delta Th/(2U_{av}^2)$
$S_{+,-}$	sorting function of thermal-plume method [—]
S_i	sorting function of u–v quadrant method [—]
T	time-averaged temperature [K]
T_c	temperature at cooled wall [K]
T_h	temperature at heated wall [K]
ΔT	temperature difference, $T_h - T_c$ [K]
t	time [s]
U	time-averaged velocity [m s^{-1}]
U_{av}	velocity averaged over the fluid layer [m s^{-1}]
U_{max}	maximum velocity [m s^{-1}]
u	longitudinal velocity fluctuation [m s^{-1}]
u'	intensity of u [m s^{-1}]
v	vertical velocity fluctuation [m s^{-1}]
v'	intensity of v [m s^{-1}]
w	spanwise velocity fluctuation [m s^{-1}]
w'	intensity of w [m s^{-1}]
x	coordinate in the streamwise direction [m]
y	coordinate in the vertical direction normal to the cooled wall [m]
z	coordinate in the spanwise direction [m].

Greek symbols

β	thermal expansion coefficient [K^{-1}]
θ	temperature fluctuation [K]
θ'	intensity of θ [K]
ν	kinematic viscosity [m^2 s^{-1}].

Other symbol

$\langle\ \rangle$	conditionally-averaged value.

between bursting period and stratification degree was also proposed. On the viewpoint of structural change of turbulence, however, these results should be discussed in more detail because the turbulent transport processes depend significantly on the organized or large-scale turbulent motion.

On the other hand, it has been well known for a long time that the so-called Bénard cells are formed in the fluid layer heated from below between parallel plates. In the presence of a forced flow, the cells change into longitudinal vortex rolls with their axes in the forced-flow direction (e.g. Mori and Uchida [21]). At relatively low Rayleigh number, less than about five times the critical one under the super-critical condition, the vortex rolls maintain their shape in stable and regular form [22, 23]. These longitudinal vortices have been observed in a laminar flow at low Reynolds number. Even in turbulent flows at high Reynolds number, the evidence of occurrence of turbulent longitudinal vortices in considerably large scale was also reported in the previous paper at very high Rayleigh number [24]. This showed that the vortical motion, which was formed intermittently, was the main contributor for vertical transport of momentum and heat. Knowledge of the inner structure of the turbulent longitudinal vortices is required to understand the transport mechanics of unstably-stratified flows, e.g. environmental turbulent-diffusion mechanics in the atmospheric boundary layer, and also to establish the numerical modeling of the stratified turbulent flows.

In the present work, three components of velocity fluctuation and temperature fluctuation are measured in strongly-unstably stratified turbulent flows between horizontal parallel plates, in which the flow and temperature fields are fully developed. The aims of the paper are to investigate the conditional-sampling techniques to detect the large-scale turbulent longitudinal vortex, and to discuss its fine structure and the mechanics of heat and momentum transfers on the basis of the conditional measurements.

2. EXPERIMENTAL

The facility used in the present study consists of a long rectangular duct originally designed in ref. [16]. The main features of the apparatus will be described here. A rectangular duct used as the test section is 0.5 m wide, 0.065 m high and 8.0 m long. Two parallel plates as heat-transfer surfaces, which are made of polished brass, can be controlled at uniform but different temperatures by flowing constant-temperature water or steam through the jackets attached behind each plate. In the present study, the temperature of the upper heat-transfer surface was maintained lower than that of the lower surface in order to establish the unstably-stratified condition. Tripping the boundary layer at the entrance of the test section facilitates the development of flow and temperature fields. The fluid used here was air.

Measurements were made 7.2 m downstream from the entrance of the duct, where the flow and temperature fields could be fully developed, so that the heat flux at the measuring section was constant throughout the fluid layer between the heat transfer surfaces. Three components of instantaneous velocity, u in the streamwise direction x, v in the direction normal to the upper cold surface y, and w in the

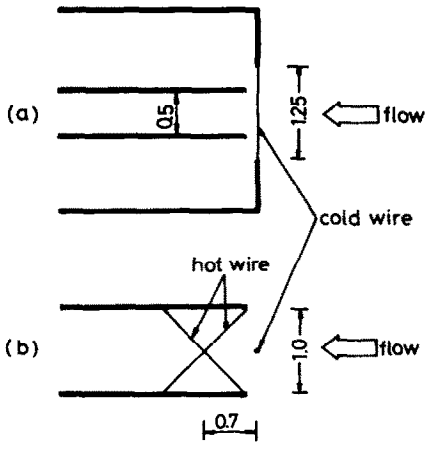

FIG. 1. Schematic of the hot and cold wire probe arrangement: (a) top view; (b) side view.

spanwise direction z, were measured with a X-hot wire probe (KANOMAX MODEL 1248-T1.5) operated by a constant-temperature anemometer (KANOMAX MODEL 1010) and the temperature with an I-cold wire probe (DISA 55P05) operated by a constant-current anemometer (DISA 55M20). The probe assembly used is shown diagrammatically in Fig. 1. The I-cold wire was set 0.7 mm upstream of the center of the X-hot wire and perpendicular to the plane of the X probe. Two components of velocity (u and v, or u and w) and temperature were measured simultaneously. The frequency response of the cold wire was estimated to be about 200 Hz from the power spectra of the temperature fluctuation, which was sufficient for the measurements. The temperature could be measured with a resolution up to 0.01 K. Experimental errors were estimated to be about $\pm 2\%$ for the mean velocity and temperature, and less than $\pm 3\%$ for r.m.s. values of turbulent fluctuations. Two hot/cold wire arrangements were used. One of them was used as a reference probe which was fixed, in most cases, at $y = 0.004$ m ($y/h = 0.0615$), where the origin of the z-coordinate was set, and the other as the sampling probe. The sampling probe position was traversed in the x-, y- and z-directions.

Analog signals from instruments were directly digitized with a 12 bit A/D converter and stored on magnetic tape. The sampling interval and recording duration were 0.0025 and 300 s, respectively, so that the sampling size for each signal was 120 000. Calculations of velocity components and temperature and statistical processing were carried out using a FACOM M-760 computer system at the Data Processing Center of Himeji Institute of Technology.

3. CONDITIONAL SAMPLING METHODS

It was expected that the ordered and large-scale motions even in the turbulent flow could be detected under the strongly unstable condition if the order motions were kept considerably steady in space and time. To gain further insight into the coherent structure of unstably-stratified turbulent flow, three conditional sampling techniques were adopted as follows.

The buoyancy effects on the turbulent structure in the thermally stratified flows are closely correlated with temperature fluctuation. The flow instability under unstable conditions should enhance the generation of the thermal plume like the Bénard convection. It is considered that the thermal plume occurs near the wall and then causes, intermittently, the large-scale turbulent thermal convection. With increasing the thermal instability, the violent thermal convection causes the structural change of the turbulence, and becomes the main contributor to organize the turbulence structure. The conditional sampling method, which is adopted here, at first intends to detect the coherent turbulence which is ordered because of the turbulent thermal plume. The signal from the sampling probe is sampled when the reference probe detects the hot or cold plume. The thermal-plume (TP) detecting method is defined by

$$\langle e_+ \rangle = \int_0^\tau e \cdot S_+ \, dt \Big/ \int_0^\tau S_+ \, dt \tag{1}$$

$$\langle e_- \rangle = \int_0^\tau e \cdot S_- \, dt \Big/ \int_0^\tau S_- \, dt \tag{2}$$

where the symbol e denotes the instantaneous fluctuations of velocity and temperature, and other arbitrary turbulent quantities at the sampling position. S_+ and S_- are the sorting functions in order to detect the hot and cold plumes, respectively, given by

$$S_+ = \begin{cases} 1; & \text{if } |\theta^2| > H\theta'^2 \quad \text{and} \quad \theta > 0 \\ 0; & \text{otherwise} \end{cases} \tag{3}$$

$$S_- = \begin{cases} -1; & \text{if } |\theta^2| > H\theta'^2 \quad \text{and} \quad \theta < 0 \\ 0; & \text{otherwise} \end{cases} \tag{4}$$

where θ is the temperature fluctuation at the reference position, θ' its intensity and H the threshold level. The terms in angular brackets in equations (1) and (2) denote the average values of the sorted samples.

The second method was a u–v plane quadrant technique which was first used by Kibens [25] and extended by Willmarth and Lu [5] in a study of the mechanics of turbulence production, namely the structure of the Reynolds stress. The signal from the sampling probe is conditionally sampled and sorted into four quadrants of the u–v plane. The method is defined as follows:

$$\langle e_i \rangle = \int_0^\tau e \cdot S_i \, dt \Big/ \int_0^\tau S_i \, dt \tag{5}$$

where

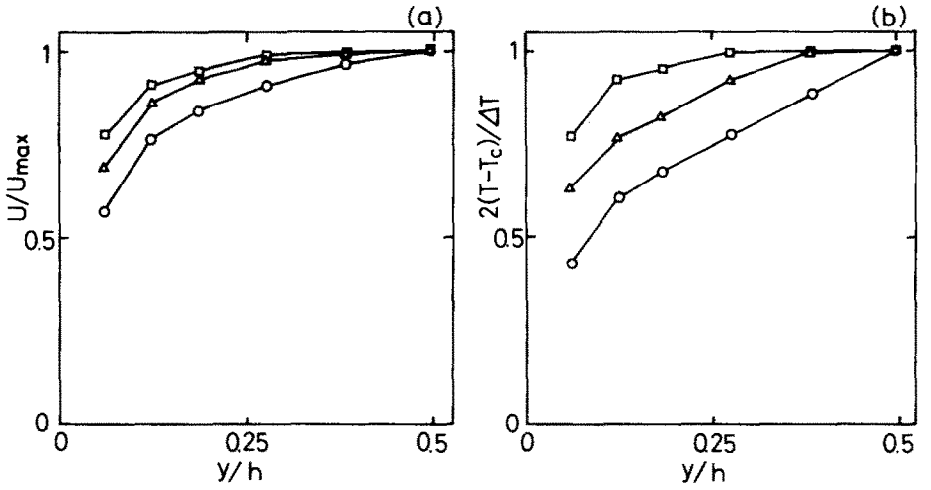

FIG. 2. Distributions of time-averaged velocity and temperature against y/h: ○, $Ri = -0.003$, $Re = 6900$; △, $\overline{Ri} = -0.111$, $Re = 6700$; □, $\overline{Ri} = -0.341$, $Re = 3800$.

$$S_i = \begin{cases} 1; & \text{if } |uv|_i > Hu'v' \text{ and the point } (u, v) \text{ in the} \\ & u\text{–}v \text{ plane belongs to the } i\text{th quadrant} \\ 0; & \text{otherwise.} \end{cases} \tag{6}$$

The third method is the variable interval time averaging (VITA) method which many investigators have used to infer the average bursting period. For a fluctuating quantity e the localized VITA variance is defined as

$$\text{var}\,(e) = (\widetilde{e^2}) - (\tilde{e})^2 \tag{7}$$

where the variable interval time average of the fluctuation is given by

$$\tilde{e} = \frac{1}{\Delta t} \int_{t-(1/2)\Delta t}^{t+(1/2)\Delta t} e \, \mathrm{d}t. \tag{8}$$

Smoothing time Δt was selected as $\Delta t u_*^2/\nu = 10$ [8, 9], where u_* is the friction velocity. The sorting function was not given, because the VITA signal was not used to detect the ordered motion but only to compare the other signals.

Using the sorting function defined by equations (3) and (4), we introduced the correlation coefficients of the fluctuations as follows. The time auto-correlation coefficient at the measuring position is defined by

$$R_{a,e}(\tau) = \langle e(t)e(t+\tau)\rangle / \langle e(t)^2\rangle. \tag{9}$$

The longitudinal spatial correlation coefficient of the turbulent quantities between the reference position ($x = 0$) and the sampling position x, which is the distance from the reference point, is defined by

$$R_{s,e}(x) = \langle e(0)e(x)\rangle / \langle e(0)^2\rangle. \tag{10}$$

The spanwise spatial correlation coefficient can be defined in the same way.

4. RESULTS AND DISCUSSION

4.1. *Time-averaged properties*

Dimensionless values of time-averaged velocity U and temperature T without conditional sampling are plotted against dimensionless distance y/h, y being the distance from the upper plate, as shown in Fig. 2. Open circles show the results for very weakly unstable flow (an approximation to neutral flow). Increasing the degree of unstable stratification, the profiles in the outer region of $y/h > 0.25$ become flatter and the gradients of the profiles near the wall become larger, so that heat and momentum are transferred more actively than those in the quasi-neutral case.

Figure 3 shows the distributions of U, T and the intensities of velocity and temperature fluctuations

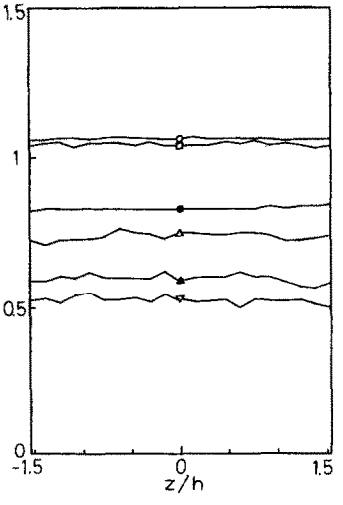

FIG. 3. Distributions of time-averaged values against spanwise direction at $y/h = 0.28$ for $\overline{Ri} = -0.111$ and $Re = 6700$: ○, U/U_{av}; ●, $(T-T_c)/\Delta T$; □, $u'/U_{av} \times 10$; ▲, $v'/U_{av} \times 10$; △, $w'/U_{av} \times 10$; ▽, $\theta'/\Delta T \times 10$.

obtained at $y/h = 0.28$ against the spanwise direction z/h. It can be seen that these time-averaged properties have no periodic behavior with respect to the z-direction.

4.2. *Relations between conditional techniques and ordered motions*

The following discussions are carried out on the basis of the measurement for $\overline{Ri} = -0.111$ and $Re = 6700$. Transient values of the velocity and temperature fluctuations and their conditional signals, which are measured by the reference probe fixed at $y/h = 0.0615$ ($yu_*/\nu = 14.8$) under the unstably-stratified condition, are shown in Fig. 4. The period assigned by A in the figure denotes the large positive fluctuation of temperature which can be detected continuously during the period, so that the condition of $S_+ = 1$ is observed intermittently but very frequently. Therefore, the temperature signal measured at the reference position shows that during the A period the hot fluid, that is, hot plume, comes up continuously from the lower hot fluid layer near the heated wall in the period. By using the TP method defined by equations (1) and (3), the transient data are averaged conditionally during this period when $S_+ = 1$. During this period, the transient signal u is seen to be held positive and v negative, and no large time variations of velocity and temperature are observed, so that the signal levels of var (u) and var (θ) are held almost at zero. As can be seen from the S_i signal obtained by using the u–v quadrant technique defined by equations (5) and (6), only the fourth quadrant ($u > 0$ and $v < 0$) can be detected most frequently in the period. These results reveal that the turbulent motion is remarkably ordered and that the ordered motion is stable during the period A. Furthermore, its structure keeps its form for a considerably long time, about 1 s.

Comparison between two signals from the reference and sampling probes is needed to understand the characteristics of the TP method and to discuss the fine structure of detected-ordered motion later. Figure 5 represents the time records of the signals from the reference probe fixed at $y/h = 0.0615$ ($y = 0.004$ m) and from the sampling probe at $y/h = 0.5$ and $z/h = 0.0$. It should be noted here that the S_i-signal is obtained from the conditional signal of sampling-probe measurement, however, θ_r and $(S_{+,-})_r$ are obtained from the reference-probe measurements. The third quadrant S_3 ($u < 0$ and $v < 0$) is observed most frequently and continuously during the period when $S_+ = 1$. The time-record signals from two probes when the sampling probe is set at $z/h = 1.38$, far away from the reference probe, are shown in Fig. 6. As seen in the figure, the first quadrant S_1 ($u > 0$ and $v > 0$) is detected frequently. Consequently, the S_i-signal from the sampling probe is found to be significantly dependent on the sampling position. It can also be expected that the order motion detected by the TP technique is large scale in space.

The TP conditional sampling was applied to detect the ordered turbulent motion. The conditionally-averaged vector fields of $\langle v_+ \rangle$–$\langle w_+ \rangle$ (when $\theta_r > 0$) and $\langle v_- \rangle$–$\langle w_- \rangle$ (when $\theta_r < 0$) with threshold level $H = 2$ is shown in Fig. 7. The reference probe is set at $y/h = 0.0615$ and the sampling probe is traversed in the y–z plane, where the total number of traversing positions is 144. The solid circle in the figure represents the position where the reference probe is fixed. A

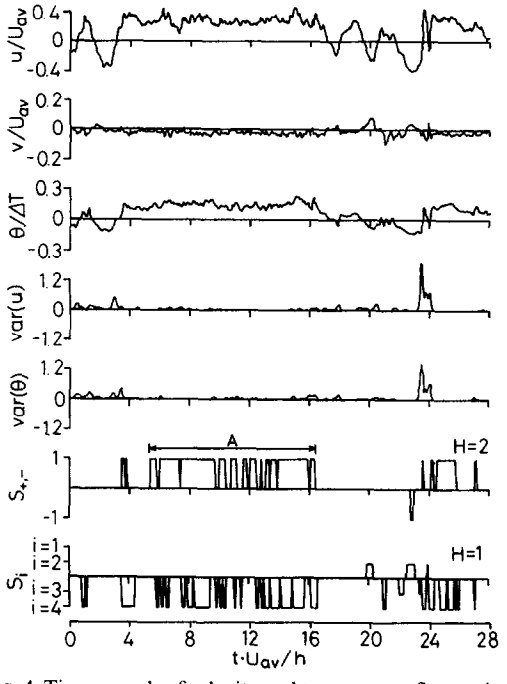

FIG. 4. Time records of velocity and temperature fluctuations and sorting functions at $y/h = 0.0615$.

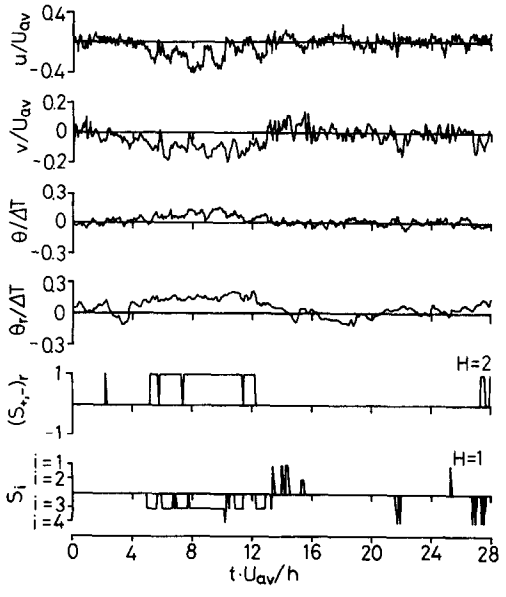

FIG. 5. Time records of velocity and temperature fluctuations and sorting functions. u, v, θ and S_i at $y/h = 0.5$; θ_r and $(S_{+,-})_r$ at $y/h = 0.0615$.

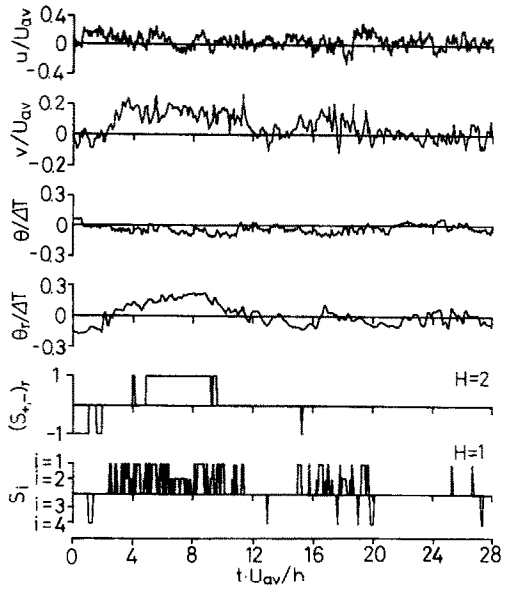

FIG. 6. Time records of velocity and temperature fluctuations and sorting functions. u, v, θ and S_i at $y/h = 0.5$ and $z/h = 1.38$; θ_r and $(S_{+,-})_r$ at $y/h = 0.0615$ and $z/h = 0.0$.

large-scale vortical structure is found to be formed between parallel plates. One of the boundaries between a pair of vortices in Fig. 7 is located in the x–y plane at $z = 0$ where the reference probe has been set. At the boundary in the $\langle v_+ \rangle$–$\langle w_+ \rangle$ vector field, the hot plume rises up from the lower plate and spreads in the spanwise direction near the wall. In the $\langle v_- \rangle$–$\langle w_- \rangle$ field, the cold plume starts to flow down from the upper cold wall near the region where the reference probe is located. The width-to-height ratio of the vortices is about 1.3. The flow patterns which were extracted for different values of threshold level H, which ranged from 1.0 to 4.0, were the same as the ones depicted in Fig. 7 except for some differences in fine structure. Hence, the threshold level for the TP method was chosen as $H = 2$. Figure 8 represents the $\langle u_+ \rangle$–$\langle v_+ \rangle$ vector field plot against the y-direction. At $y/h = 0.5$, the conditional averages show that $\langle u_+ \rangle < 0$ and $\langle v_+ \rangle < 0$ at $z/h = 0.0$ and $\langle u_+ \rangle > 0$ and $\langle v_+ \rangle > 0$ at $z/H = 1.38$, corresponding to the third and first quadrants on the $\langle u_+ \rangle$–$\langle v_+ \rangle$ plane, respectively. These quadrant numbers are in agreement with the ones which are observed most frequently during the period when $S_+ = 1$, respectively, as seen from the S_i-signals in Figs. 5 and 6, at $z/h = 0$ and 1.38.

The conditionally-averaged patterns of the v–w vectors were obtained using the u–v quadrant method defined by equations (5) and (6) with the threshold level $H = 1$. The results are shown in Fig. 9. The vortex rolls are similar in shape to ones obtained by using the TP method. The width-to-height ratio of the vortex for different events agrees with each other and is 1.3 approximately. As compared with the results under higher ($\overline{Ri} = -0.341$) and lower stratification ($Ri = -0.111$), the ratio was almost the same. Hence, we expect that if the vortex rolls were organized, by buoyancy force, sufficiently to remain stable in space and time, the width-to-height ratio of vortex roll may appear independent of the sorting technique and stratification degree. From the previous study [23] on the laminar duct-flow heated from below and under super-critical conditions, the roll width was equal to the duct height at low Rayleigh number but decreased with increasing Rayleigh number (the ratio was 0.8 at the Rayleigh number five times the critical one). In the present study, the roll width is larger than the duct height although the Grashof number is very large, i.e. 1031 times the critical Rayleigh number. This result reveals that roll width depends on flow configuration, i.e. whether flow is laminar or turbulent.

Although the locations of the vortices, which are detected using the u–v quadrant technique, depend on the quadrant of the point (u, v) in the u–v plane, the vortices have almost the same shape. This indicates that the turbulent structure both near the wall and also the outer region is organized considerably by thermal plumes and that the main contributor to produce ordered turbulent motion is buoyancy force. Accordingly, using the u–v quadrant technique, we

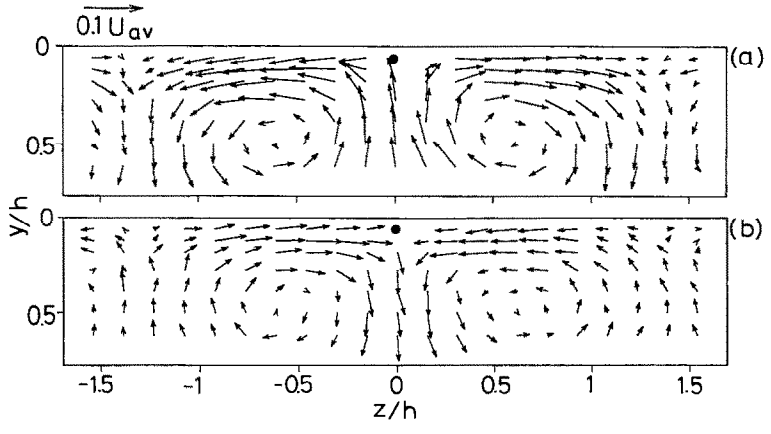

FIG. 7. Velocity vector fields, obtained with the TP method: (a) $\langle v_+ \rangle$–$\langle w_+ \rangle$; (b) $\langle v_- \rangle$–$\langle w_- \rangle$.

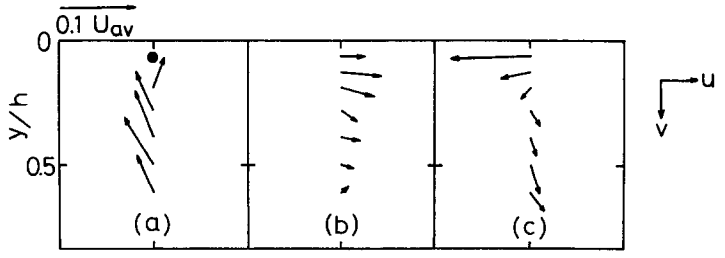

FIG. 8. Velocity vectors of $\langle u_+ \rangle$ and $\langle v_+ \rangle$, obtained with the TP method: (a) $z/h = 0.0$; (b) $z/h = 0.615$; (c) $z/h = 1.38$.

can detect the ordered motion which has already been organized in the large-scale vortical structure by thermal plume, i.e. buoyancy effect. The TP conditional technique can be applied successfully to detect the thermal plume, so that the TP method is more suitable to understand the turbulent structure of strongly and unstably stratified flow as compared with the u–v quadrant technique. In comparison the u–v quadrant technique has been useful to examine the 'bursts' mechanics near the wall under the neutral condition. As seen in Figs. 4–6, the signals from VITA processing represent that very small level in the period when the turbulence is organized in a vortical structure and that the intermittent high level is observed only at the beginning of the formation and destruction of the vortex rolls, so that the VITA technique is not adequate to detect the ordered motion described above and to discuss the turbulent mechanics in the strongly-unstably stratified turbulent flows.

4.3. *Structure of turbulent roll vortex and turbulent transport mechanics*

Figure 10 shows the spanwise spatial correlation of the v-component along the centerline between the upper and lower plates. The reference probe was set at $y/h = 0.5$ where $z/h = 0.0$ and the sampling probe was traversed horizontally in the spanwise direction at $y/h = 0.5$. It was confirmed that the three vortices exist between the side wall and the center of the duct, so that six vortices are formed in the whole region of the duct and the flow pattern detected here is an array of longitudinal vortices. The apparent flow pattern

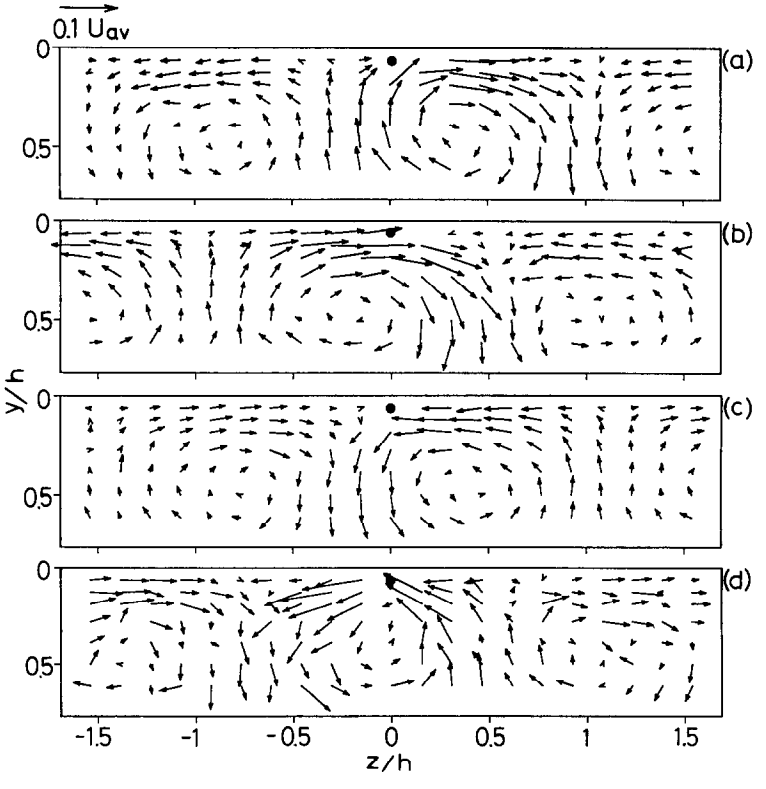

FIG. 9. Velocity vectors of $\langle v_i \rangle$ and $\langle w_i \rangle$, obtained with the u–v quadrant method: (a) $u_r > 0$ and $v_r > 0$; (b) $u_r < 0$ and $v_r > 0$; (c) $u_r < 0$ and $v_r < 0$; (d) $u_r > 0$ and $v_r < 0$.

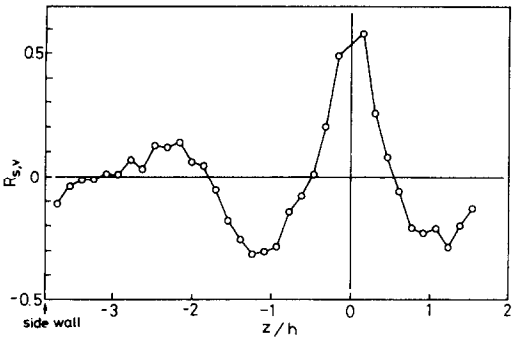

FIG. 10. Conditional space-correlation with respect to the spanwise direction of v. Reference probe is fixed at $y/h = 0.5$.

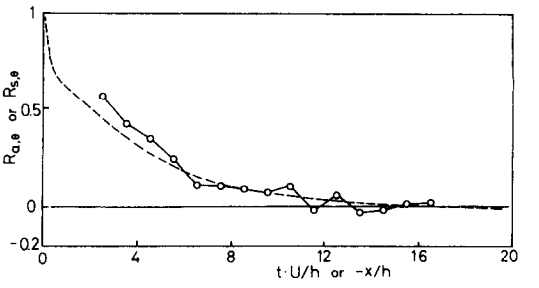

FIG. 11. Conditional auto- and space-correlations at $y/h = 0.0615$: ———, auto-correlation; ○, space-correlation.

observed here is very similar to the longitudinal vortex alignment which occurred in the laminar flow between parallel plates heated from below at Rayleigh numbers above the critical value [22, 23]. However, the details of velocity and temperature profiles and the transport mechanics are significantly different from the ones in the laminar flow. The correlation values rapidly decreased near the side wall. This suggests that the effects of the aspect ratio of the duct are so small that the vortices near the side wall have no significant influence on the structure of the vortices which are detected near the reference probe.

The time auto-correlation and the spatial correlation in the x-direction which are calculated at $y/h = 0.0615$ and $z/h = 0$ from equations (9) and (10) are compared in Fig. 11. It can be seen that the longitudinal spatial correlation compares well with the auto-correlation. The reductions of the two correlations with $-x/h$ or tU/h are considerably slow, so that those correlation levels are observed to be relatively high even at $-x/h = 6$ or $tU/h = 6$. It is

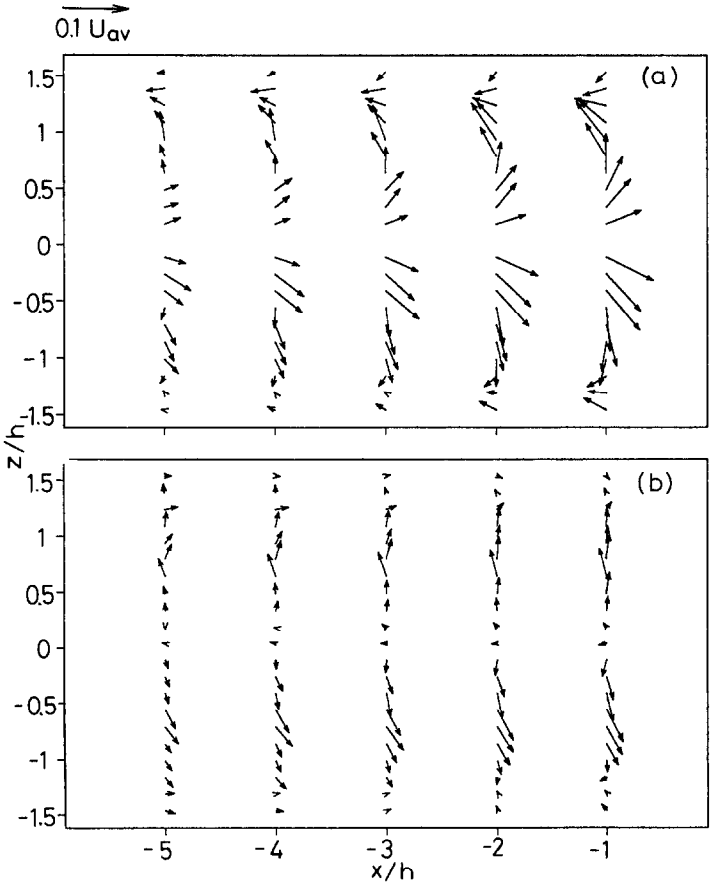

FIG. 12. Velocity vectors of $\langle u_+ \rangle$ and $\langle w_+ \rangle$, obtained with the TP method: (a) $y/h = 0.12$; (b) $y/h = 0.28$; (c) $y/h = 0.5$; (d) $y/h = 0.62$.

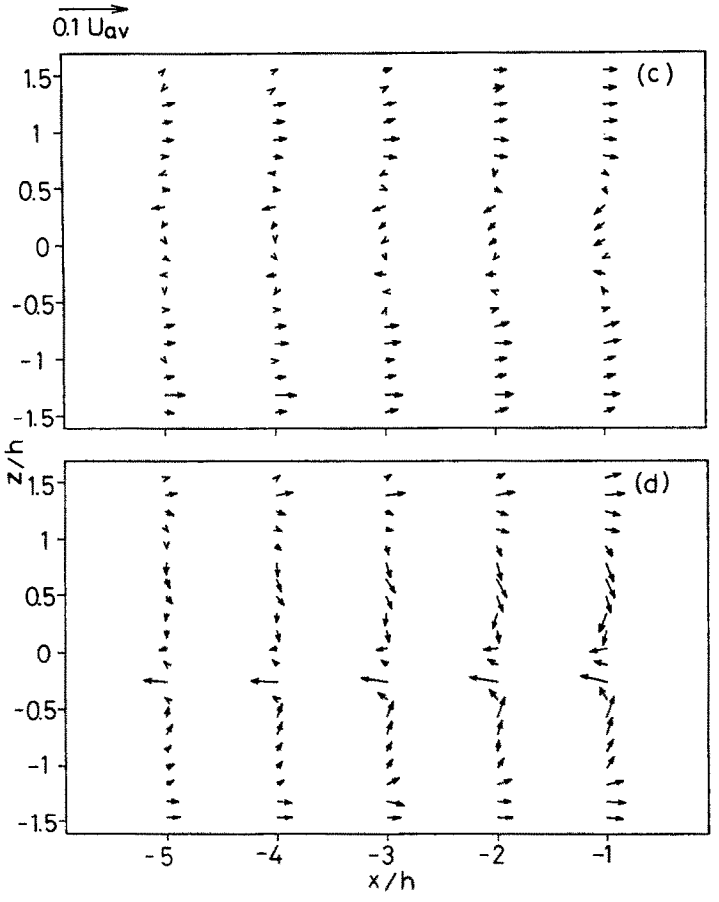

FIG. 12 (*Continued*).

expected that the vortical flow pattern can be recognized in the upstream and downstream region from the reference point, when the large-scale turbulent vortex rolls have been detected at the reference point of $y/h = 0.0615$ using the TP method. The so-called Taylor hypothesis is adopted here to investigate the streamwise structure of the turbulent vortex roll since a good agreement between space- and auto-correlations was observed. Figures 12 and 13 depict the $\langle u_+ \rangle$–$\langle w_+ \rangle$ and $\langle u_+ \rangle$–$\langle v_+ \rangle$ vector fields, respectively, which are calculated by the TP method in the case of $S_+ = 1$ at the reference point of $y/h = 0.0615$. As discussed above, the streamwise distances from the reference point were not measured directly but estimated from the data at $x/h = 0.0$ by using Taylor's hypothesis, i.e. by converting time-lag into the streamwise distance by means of local time-mean velocity without conditional sampling U. Although the application of this hypothesis to this type of flow configuration is debatable, it might only be said that a similar flow pattern existed up- and downstream when such a pattern was detected at $x/h = 0.0$. These longitudinal vortex rolls were recognized in the streamwise extent of $-6 \leqslant x/h \leqslant 5$ at $\overline{Ri} = -0.111$ and $-9 \leqslant x/h \leqslant 7$ for strongly stratified flow at $\overline{Ri} = -0.341$.

The detailed structure of the turbulent longitudinal vortex which has been detected using the TP method is discussed as follows. Figure 14 shows the contour plots of the conditional averages of the three velocity components and temperature in the case of $S_+ = 1$ with $H = 2$. The velocity components were non-dimensionalized by the cross-sectional mean velocity U_{av} and the temperature by the temperature difference of the upper and lower plates ΔT. As seen in the $\langle v_+ \rangle$ contour plot, the negative peak is observed at the upwelling boundary of vortices, namely $z/h = 0.0$, where the hot plume heated at the lower hot wall flows upwards to the upper cold plates. The positive peak exists at the downwelling boundary, $z/h = \pm 1.3$, where the cold plume cooled at the upper plate flows downwards to the lower plate. The feature of the hot and cold plume motions can be also seen in the $\langle \theta_+ \rangle$ contour plot. Near the upper wall, the $\langle u_+ \rangle$ contour has a positive peak at the upwelling boundary, and on the right-hand side of the upwelling boundary the $\langle w_+ \rangle$ contour has positive and on the left-hand side negative peaks. Near the upwelling boundary, accordingly, the hot plume from the lower plate impinges upon the upper plate and spreads laterally. It also accelerates the primary flow ($\langle u_+ \rangle > 0$) near the upper wall. At the other boundaries (i.e. $z/h = \pm 1.3$), the cold plume from the upper plate blocks the primary flow ($\langle u_+ \rangle < 0$).

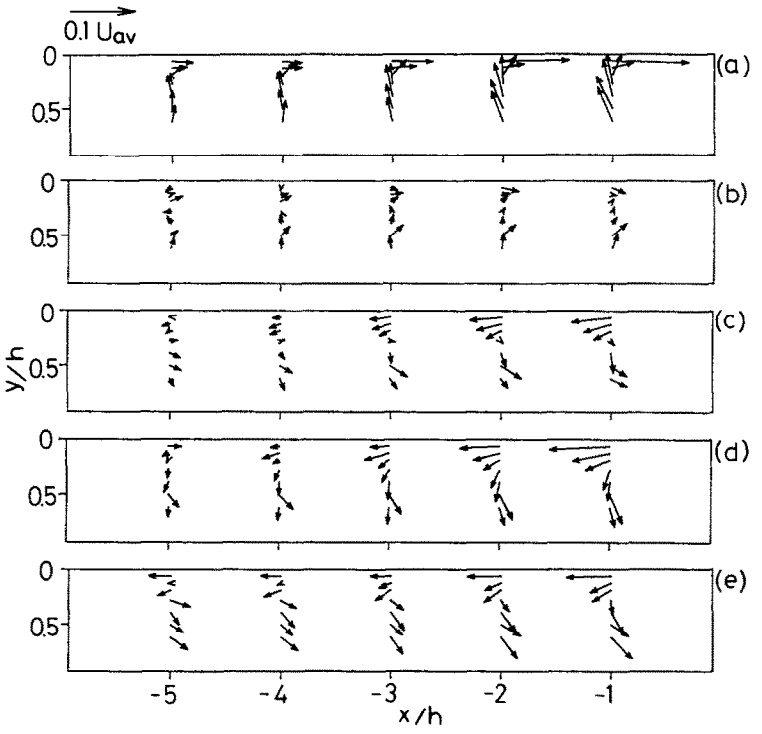

FIG. 13. Velocity vectors of $\langle u_+ \rangle$ and $\langle v_+ \rangle$, obtained with the TP method: (a) $z/h = -0.15$; (b) $z/h = -0.46$; (c) $z/h = -0.77$; (d) $z/h = -1.08$; (e) $z/h = -1.38$.

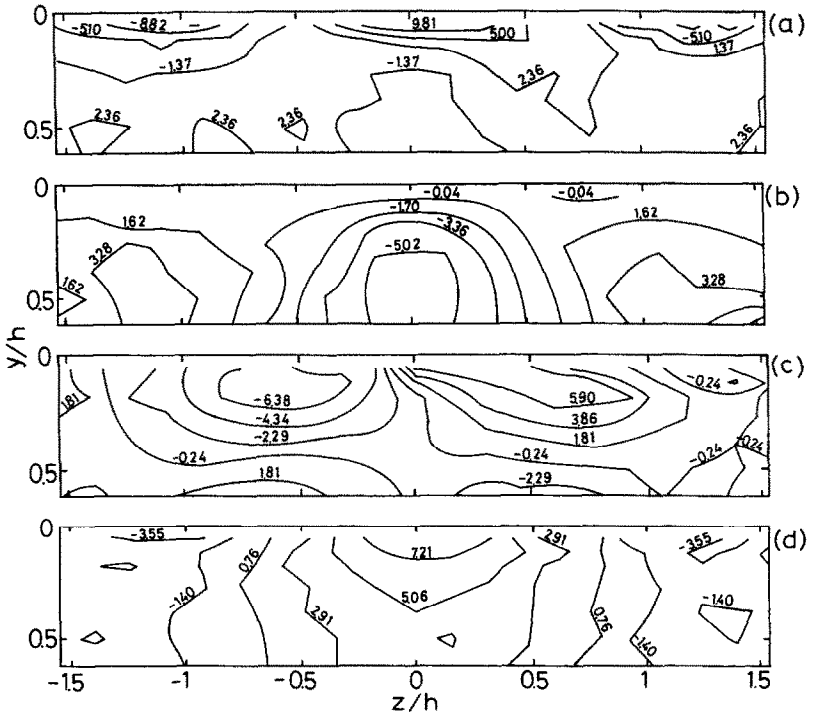

FIG. 14. Contours of $\langle u_+ \rangle$, $\langle v_+ \rangle$, $\langle w_+ \rangle$ and $\langle \theta_+ \rangle$, obtained with the TP method: (a) $\langle u_+ \rangle / U_{av} \times 100$; (b) $\langle v_+ \rangle / U_{av} \times 100$; (c) $\langle w_+ \rangle / U_{av} \times 100$ and $\langle \theta_+ \rangle / \Delta T \times 100$.

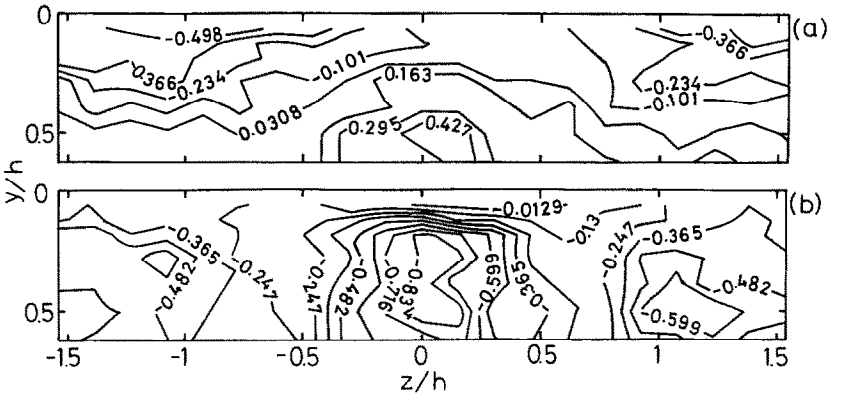

FIG. 15. Contours of conditional turbulent transfer rates of momentum and heat, obtained with the TP method: (a) $\langle uv_+\rangle/u'v'$; (b) $\langle v\theta_+\rangle/v'\theta'$.

This secondary flow caused by the regular plume alignment constitutes the longitudinal-vortex pairs.

Figure 15 shows the contours of turbulent transfer rates of momentum ($\langle uv_+\rangle/u'v'$) and heat ($\langle v\theta_+\rangle/v'\theta'$). At the boundary of $z/h = 0$, the values of $\langle uv_+\rangle/u'v'$ are positive near the center of the duct, however, they become negative in the vicinity of the upper wall. As seen in the $\langle u_+\rangle$ and $\langle v_+\rangle$ contour plot in Fig. 14, the sign of $\langle u_+\rangle$ changed from plus to minus in the y-direction at that boundary, but the sign of $\langle v_+\rangle$ was unchanged, i.e. minus, due to the upward active convection caused by the buoyancy force. The characteristics of $\langle uv_+\rangle/u'v'$ are dependent essentially on the longitudinal vortical structure. The values of $\langle v\theta_+\rangle/v'\theta'$ are negative in a whole region. A negative peak was observed nearby at $y/h = 0.5$ and $z/h = 0$ where the heated fluid is transferred upward violently. The absolute values of $\langle v\theta_+\rangle/v'\theta'$ are small at the center of the vortex roll, approximately $y/h = 0$ and $z/h = \pm 0.6$, so that the thermal hot plume at the boundary is the main contributor to turbulent heat transfer.

Dimensionless velocity and temperature profiles obtained from conditional averages using the TP method are plotted against dimensionless distance y/h in Fig. 16, where the conditional averages have been carried out at $z/h = 0.0$, 0.615 and 1.38, considered as at two boundaries and the center of the vortex rolls, respectively. In the region of $0.25 < y/h < 0.4$ at $z/h = 0$ (at the upwelling boundary) the counter-gradient turbulent diffusion of momentum occurs, because in this region the velocity gradient is positive, while $\langle uv_+\rangle/u'v'$ is also positive (see Fig. 15). In the region nearby at $y/h = 0.5$ and $z/h = 0$ where $\langle uv_+\rangle/u'v'$ is positive, however, no counter-gradient diffusion can be observed since the velocity gradient is negative. In the region of $0.4 < y/h < 0.5$ at $y/h = 0.615$ (near the center of the vortex), both the temperature gradient and $\langle v\theta_+\rangle/v'\theta'$ are negative, so that in this region the counter-gradient diffusion of heat occurs. Incidently, in laminar longitudinal vortical flow at low Reynolds number, the counter-gradient profile of temperature was observed near the center of the vortex under considerably high Rayleigh number [22].

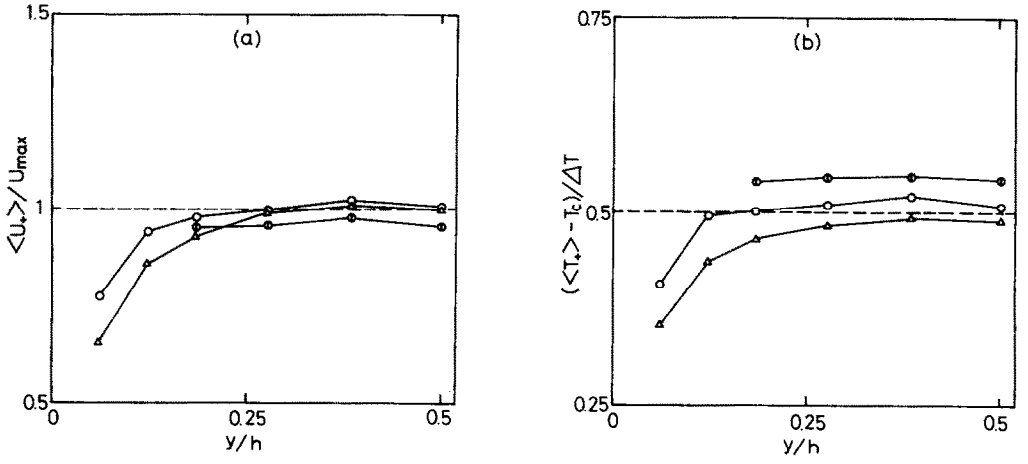

FIG. 16. Distributions of $\langle U_+\rangle$ and $\langle T_+\rangle$, obtained with the TP method: ⊕, $z/h = 0.0$; ○, $z/h = 0.615$; △, $z/h = 1.38$.

5. CONCLUSIONS

The large-scale coherent structure in fully-developed stratified turbulent flow in a duct with an aspect ratio of 7.7 under the unstable condition, has been experimentally investigated by using both the conditionally-averaging and two-point measuring techniques. Correlations between conditionally-averaging techniques and the detected coherent structures have been discussed. The main results obtained from the present work are summarized as follows.

(1) Under the unstable condition, active generation of turbulent thermal plumes are caused by buoyancy force. The thermal plumes become the main contributors to organize the turbulent structure. Accordingly, the TP detecting technique is proposed in order to identify the coherent structure in the unstably-stratified flow and to investigate its turbulent mechanics.

(2) The turbulent structure under the strongly unstable condition is essentially different from that in the neutral flow. Unstable buoyancy effects cause the large-scale coherent structure in the form of longitudinal vortex-roll array. The array fills the whole region in a duct, so that six vortical rolls are formed in the duct. The observed vortex rolls are remarkably stable in space and time. The width of the vortex rolls, which are detected near the center of the duct, is 1.3 times the duct height.

(3) The structure of the turbulent longitudinal vortex detected here as essentially different from the longitudinal vortex which, as well known, has been observed in laminar flow between parallel plates heated from below. The turbulent transports of heat and momentum are controlled by the coherent longitudinal vortices, because the vortices occur intermittently but frequently and maintain their form for a long interval. When the turbulent structure is organized in vortical form, the counter-gradient turbulent transport of heat and momentum is observed.

REFERENCES

1. S. J. Kline, W. C. Reynolds, F. A. Schraub and P. W. Runstadler, The structure of turbulent boundary layers, *J. Fluid Mech.* **30,** 741–773 (1967).
2. E. R. Corino and R. S. Brodkey, A visual investigation of the wall region in turbulent flow, *J. Fluid Mech.* **37,** 1–30 (1969).
3. H. T. Kim, S. J. Kline and W. C. Reynolds, The production of turbulence near a smooth wall in a turbulent boundary layer, *J. Fluid Mech.* **50,** 133–160 (1971).
4. A. J. Grass, Structural features of turbulent flow over smooth and rough boundaries, *J. Fluid Mech.* **50,** 233–255 (1971).
5. W. W. Willmarth and S. S. Lu, Structure of the Reynolds stress near the wall, *J. Fluid Mech.* **55,** 65–92 (1972).
6. S. S. Lu and W. W. Willmarth, Measurements of the structure of the Reynolds stress in a turbulent boundary layer, *J. Fluid Mech.* **60,** 481–511 (1973).
7. J. M. Wallace, H. Eckelmann and R. S. Brodkey, The wall region in turbulent shear flow, *J. Fluid Mech.* **54,** 39–48 (1972).
8. R. F. Blackwelder and R. E. Kaplan, On the wall structure of the turbulent boundary layer, *J. Fluid Mech.* **76,** 89–112 (1976).
9. R. F. Blackwelder and J. H. Haritonidis, Scaling of the bursting frequency in turbulent boundary layers, *J. Fluid Mech.* **132,** 87–103 (1983).
10. D. A. Shah and R. A. Antonia, Scaling of the "bursting" period in turbulent boundary layer and duct flows, *Physics Fluids* **A1**(2), 318–325 (1989).
11. S. P. S. Arya, Buoyancy effects in a horizontal flat-plate boundary layer, *J. Fluid Mech.* **68,** 321–343 (1975).
12. S. Komori, H. Ueda, F. Ogino and T. Mizushina, Turbulence structure in unstably-stratified open-channel flow, *Physics Fluids* **25**(9), 1539–1546 (1982).
13. T. Mizushina, F. Ogino and N. Katada, Ordered motion of turbulence in a thermally stratified flow under unstable condition, *Int. J. Heat Mass Transfer* **25,** 1419–1425 (1982).
14. C. J. H. Nicholl, Some dynamical effects of heat on a turbulent boundary layer, *J. Fluid Mech.* **40,** 361–384 (1970).
15. A. A. Townsend, Mixed convection over a heated horizontal plane, *J. Fluid Mech.* **55,** 209–227 (1972).
16. K. Fukui, Buoyancy effects on transport phenomena, Ph.D. Dissertation, Kyoto University (1982).
17. K. Fukui, M. Nakajima and H. Ueda, A laboratory experiment on momentum and heat transfer in the stratified surface layer, *Q. J. R. Met. Soc.* **109,** 661–676 (1983).
18. J. A. Businger, J. C. Wyngaard, Y. Izumi and E. F. Bradley, Flux-profile relationships in the atmospheric surface layer, *J. Atmos. Sci.* **28,** 181–189 (1971).
19. H. Ueda, S. Komori and K. Fukui, A laboratory experiment on lateral diffusion of scalar quantities in the stratified surface layer, *Atmos. Environment* **20,** 757–762 (1986).
20. K. Fukui and M. Nakajima, Unstable stratification effects on turbulent shear flow in the wall region, *Int. J. Heat Mass Transfer* **28,** 2343–2352 (1985).
21. Y. Mori and Y. Uchida, Forced convective heat transfer between horizontal flat plates, *Int. J. Heat Mass Transfer* **9,** 803–817 (1966).
22. K. Fukui, M. Nakajima and H. Ueda, The longitudinal vortex and its effects on the transport processes in combined free and forced laminar convection between horizontal and inclined parallel plates, *Int. J. Heat Mass Transfer* **26,** 109–120 (1983).
23. K. Fukui, Longitudinal vortices in mixed convection in a horizontal duct, *Kagaku Kogaku Ronbunshu* **15,** 963–967 (1989).
24. H. Ueda, S. Komori and K. Fukui, Large-scale vortical structure in the turbulent boundary layer flow under unstably-stratified conditions. In *Transport Phenomena in Turbulent Flows* (Edited by M. Hirata and N. Kasagi), pp. 325–333. Hemisphere, Washington, DC (1988).
25. V. Kibens, The intermittent region of a turbulent boundary layer, Ph.D. Dissertation, The Johns Hopkins University (1968).

STRUCTURE COHERENTE DE TOURBILLONS LONGITUDINAUX TURBULENTS DANS UN ECOULEMENT STRATIFIE INSTABLE

Résumé—La structure cohérente à large échelle dans un écoulement turbulent à densité stratifiée, soumis à des conditions fortement instables est étudiée expérimentalement en utilisant quelques techniques d'échantillonnage conditionnel. Un arrangement de rouleaux longitudinaux de grande échelle peut être reconnu en utilisant la nouvelle technique d'échantillonnage conditionnel, c'est le panache thermique détectant le sillage chaud ou froid à la frontière des rouleaux ordonnés turbulents. Les mesures donnent une connaissance détaillée de la fine structure de la turbulence et des mécanismes du transfert turbulent de chaleur et de quantité de mouvement.

DIE KOHÄRENTE STRUKTUR VON TURBULENTEN LÄNGSWIRBELN IN EINER INSTABIL GESCHICHTETEN TURBULENTEN STRÖMUNG

Zusammenfassung—Die makroskopisch kohärente Struktur in einer dichtegeschichteten turbulenten Strömung wird unter stark instabilen Bedingungen experimentell untersucht. Unter Verwendung einer neuen Technik wird eine Anordnung von großräumigen, längsgerichteten Wirbelwalzen entdeckt. Bei dem Verfahren wird die heiße oder kalte Auftriebsfahne am Rande von geordneten turbulenten Walzen separiert. Das Meßverfahren liefert die detaillierte Kenntnis der Feinstruktur der Turbulenz und der Mechanismen der turbulenten Wärme- und Impulsübertragung.

КОГЕРЕНТНАЯ СТРУКТУРА ТУРБУЛЕНТНЫХ ПРОДОЛЬНЫХ ВИХРЕЙ В ТУРБУЛЕНТНОМ ПОТОКЕ С НЕУСТОЙЧИВОЙ СТРАТИФИКАЦИЕЙ

Аннотация—С использованием методов условной выборки экспериментально исследуется крупномасштабная когерентная структура турбулентного потока со стратификацией плотности в условиях сильной неустойчивости. Расположение крупномасштабных продольных вихревых валов может быть установлено с помощью нового метода условной выборки, а именно, метода обнаружения тепловых струй, который позволяет выделитв нагретую или ненагретую тепловую струю на границе упорядоченных турбулентных валов. Измерения, выполненные с использованием метода условной выборки, дают подробную информацию о тонкой структуре турбулентности и механике турбулентного переноса тепла и количества движения.